

Integrated Combination Treatment Using a “Smart” Chemotherapy and MicroRNA Delivery System Improves Outcomes in an Orthotopic Colorectal Cancer Model

Hai-Jun Liu, Xin Luan, Hai-Yi Feng, Xiao Dong, Si-Cong Yang, Zhong-Jian Chen, Qin-Yi Cai, Qin Lu, Yunpeng Zhang, Peng Sun, Mei Zhao,* Hong-Zhuan Chen, Jonathan F. Lovell, and Chao Fang*

Mesoporous silica nanoparticles (MSN) can load and deliver potentially synergistic anticancer agents such as small molecule cytotoxics (like doxorubicin, DOX) and nucleic acids (like microRNA, miRNA). However, these cargos have different underlying chemical properties so overcoming respective intracellular delivery barriers is a key consideration. Strategies to deliver DOX from MSN frequently employ pH-driven mechanisms that are restricted to the acidic environment of lysosomes. Conversely, strategies to deliver miRNA make use of approaches that deliberately compromise lysosomal membrane integrity to enable cytosolic delivery of the payload. To reconcile these two needs (lysosomal delivery of DOX and intracellular delivery of miRNA), a new methodology by “weaving” polyethylenimine on the MSN surface through disulfide bonds to achieve superior delivery of chemotherapy (DOX) and miRNA therapy (using miRNA-145) is developed. Furthermore, an active targeting strategy based on a peptide ligand with affinity to glucose-regulated protein 78 (GRP78), a cell surface protein overexpressed in colorectal carcinoma, is developed. The active targeting approach results in enhanced synergistic antitumor effect both *in vitro* and *in vivo* in an orthotopic murine model of colorectal cancer. Taken together, this work demonstrates the capability and advantages of “smart” MSN delivery systems to deliver anticancer cargo appropriately to targeted cancer cells.

1. Introduction

Nanocarrier-mediated codelivery of chemotherapeutics and nucleic acids which target independent molecular pathways has demonstrated potential in improving the therapeutic outcomes of cancer.^[1] With distinct physicochemical properties (e.g., size, stability, solubility, etc.), developing single codelivery systems for small molecule drug and nucleic acids is a challenge.^[1b,c,2]

For successful dual-drug loading of small molecule drugs and nucleic acids, various nanocarriers have been developed, including cationic micelles, self-assembled cationic peptides, cationic liposomes, as well as the functionalized inorganic nanomaterials (mesoporous silica nanoparticles (MSN) and graphene oxide).^[1b,c,2,3] Although stimuli-responsive design has been developed for on-demand release of gene or chemotherapeutics,^[4] few reports have been focused to discuss the release kinetics influenced by the interaction of the two agents. One earlier work clearly

H.-J. Liu, X. Luan, H.-Y. Feng, X. Dong, S.-C. Yang, Z.-J. Chen, Q.-Y. Cai, Q. Lu, Prof. H.-Z. Chen, Prof. C. Fang
Hongqiao International Institute of Medicine
Shanghai Tongren Hospital and Department of Pharmacology and Chemical Biology
Institute of Medical Sciences
Shanghai Jiao Tong University School of Medicine (SJTU-SM)
280 South Chongqing Road, Shanghai 200025, China
E-mail: fangchao32@sjtu.edu.cn
Y. Zhang, Dr. P. Sun
Department of General Surgery
Shanghai Tongren Hospital
SJTU-SM
1111 Xianxia Road, Shanghai 200336, China

Prof. M. Zhao
Department of Pharmacy
Shanghai University of Medicine and Health Sciences
279 Zhouzhu Road, Shanghai 201318, China
E-mail: zhaom@sumhs.edu.cn
Prof. J. F. Lovell
Department of Biomedical Engineering
University at Buffalo
State University of New York
Buffalo, NY 14260, USA

 The ORCID identification number(s) for the author(s) of this article can be found under <https://doi.org/10.1002/adfm.201801118>.

DOI: 10.1002/adfm.201801118

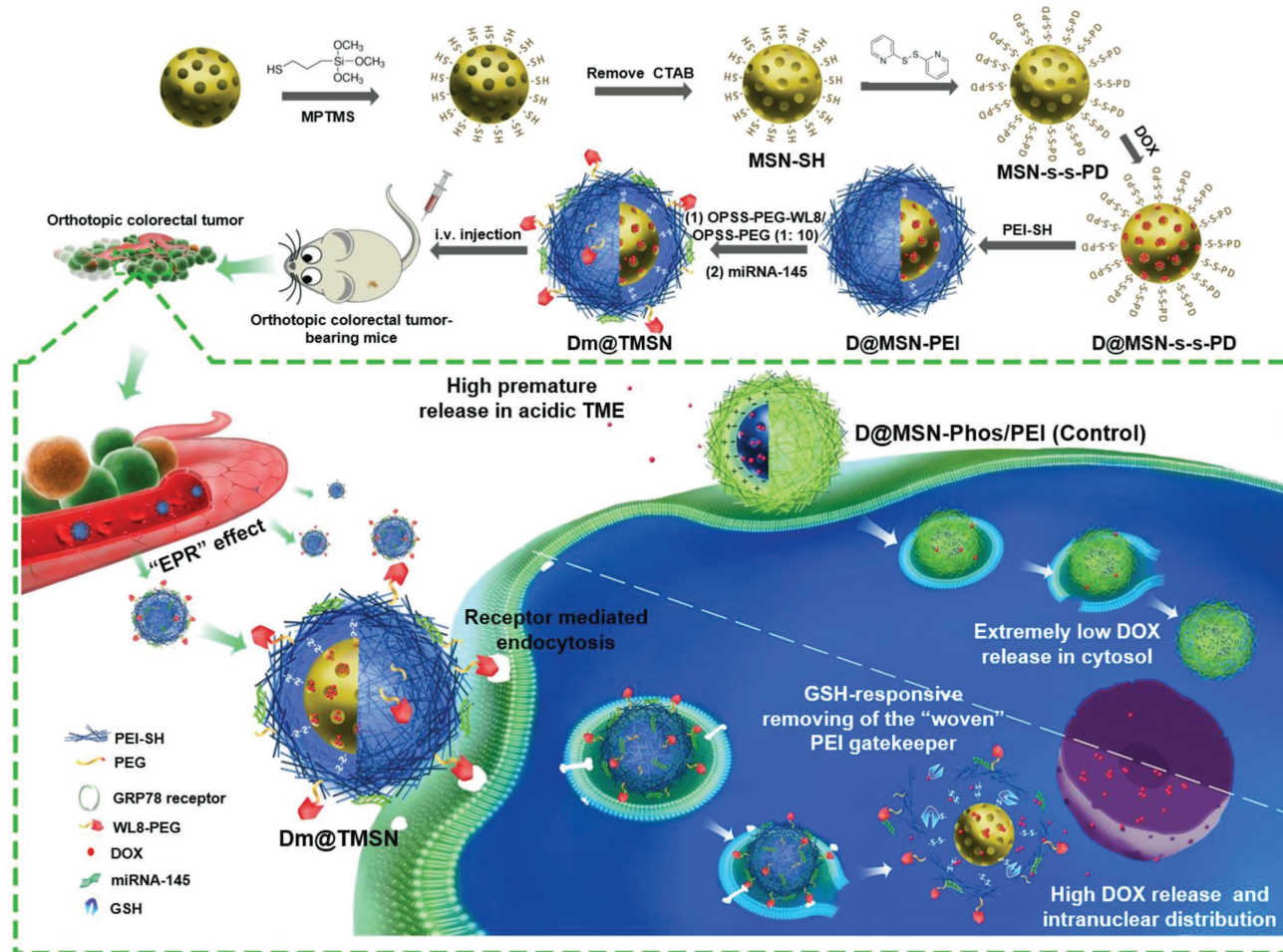


Figure 1. Schematic illustration of the preparation (top) and proposed mechanism (bottom) of the MSN-based DOX and miRNA-145 smart delivery system.

demonstrated that hydrogen bonding interactions between the drug (5-FU) and gene (antisense oligonucleotides) adversely affected the release profiles of the individual agents from the codelivery system, which may compromise the effect of combination therapy.^[5]

To the best of our knowledge, counter-productive interactions generated from intracellular, compartment-dependent delivery and release of two distinct therapeutic molecules have not been addressed in detail yet. This problem is particularly prominent in recent reports using MSN as the codelivery nanocarrier. Specifically, rapid lysosomal escape is required for nanoparticles to achieve gene delivery into the cytosol, which is the site of action. However, this requirement can sometimes be disadvantageous for drug release, especially when drug release is dependent on the acidic compartment of lysosomes. Previously, a series of reports described the development of phosphonate and polyethylenimine (PEI) functionalized MSN (MSN-Phos/PEI).^[4c,d,6] The authors electrostatically bound doxorubicin (DOX) to the porous interior to acquire high drug loading and meanwhile cationic PEI was bound to the exterior, endowing the MSN to codeliver DOX and P-gp siRNA. Unfortunately, DOX release only occurred in acidic lysosomes ($\text{pH} \approx 5$) caused

by proton interference, and there was nearly none in neutral cytosol condition ($\text{pH} \approx 7.4$) due to the strong binding of DOX and phosphonate.^[4c] It can be expected that after rapid lysosomal escape of the nanoparticles into the cytosol for siRNA delivery, further DOX release was limited. This can be seen with confocal laser scanning microscopy (CLSM); even after 3 d incubation with cancer cells (KB-V1), a substantial amount of DOX was still confined in the nanoparticles in the cytosol, although DOX is only active and able to exert cytotoxic effects following translocation to the nucleus.^[4c] Similar release behaviors were also reported using phosphonate-modified MSN,^[7] hollow MSN,^[8] and in recent work using anionic 3-isocyanatopropyltriethoxysilane (ICP) modified MSN for DOX and PKM2 siRNA codelivery.^[9] Limited DOX release from the carrier to the tumor cells limits the impact of combination therapy.^[10]

To overcome these challenges, we present a MSN delivery system codelivery of DOX and a nucleic acid (miRNA-145) (Figure 1). DOX is conventionally loaded in the pores of the MSN as previously described.^[11] Instead of using a phosphonate group to electrostatically bind PEI, we directly wove PEI (molecular weight of 1.8 kDa) onto the MSN surface via a reduction-sensitive disulfide linkage, for miRNA condensation.

The woven PEI on the MSN surface acts as a gatekeeper to prevent premature release of DOX at neutral pH of body fluids and within the tumor microenvironment (TME, pH 6.5–6.8)^[12] prior to nanoparticle uptake by tumor cells. The nanoparticles can then quickly escape from the lysosome into the cytosol for miRNA-145 delivery, mediated by the proton sponge effect of PEI.^[13] Then, the reducing environment ($0.5\text{--}10 \times 10^{-3}$ M glutathione/GSH) within tumor cells^[14] hydrolyzes the disulfide bond to remove the PEI gatekeeper from the MSN surface, resulting in release of DOX from the carrier. This design for MSN-based codelivery of DOX and nucleic acids can provide for optimal functional delivery of both cargos.

MicroRNAs (miRNAs) are 20–23 nucleotides long and act as regulators of posttranscriptional gene expression for a broad set of target genes. Aberrant expression profiles of miRNAs in cancer make them good therapeutic targets. Restoration of downregulated miRNA or inhibition of overexpressed miRNA is the basis of miRNA-based therapy.^[15] Previous study demonstrated that miRNA-145 was downregulated in clinical human colon cancer tissues, and negatively correlated with p70S6K1, an important signaling protein for regulating cellular functions.^[16] Further investigation showed miRNA-145 can inhibit p70S6K1 post-transcriptional expression by binding to its 3'-UTR. Then, its downstream angiogenic factors, hypoxia-inducible factor 1 α (HIF-1 α) and vascular endothelial growth factor (VEGF), are efficiently suppressed. These events finally lead to the inhibition of tumor angiogenesis and growth.^[16] Here, we codelivered DOX and miRNA-145 to combine chemotherapy with nucleic acid based antiangiogenic therapy in an orthotopic colorectal tumor model. Targeting angiogenesis in combination with chemotherapy is consistent with approved clinical practice in the treatment of colorectal cancer patients.^[17]

We further used WL8 peptide (WIFPWIQI)-capped polyethylene glycol (PEG) to confer the nanoparticles both the stealth and tumor cell targeting property. The WL8 peptides are high avidity ligands which target glucose-regulated protein-78 (GRP78)^[18] overexpressed on the surface of colorectal cancer cell such as SW480.^[19] The enhanced synergistic antitumor efficacy of the DOX and miRNA-145 loaded, targeted MSN (Dm@TMSN) was evaluated both in vitro and in vivo in an orthotopic SW480 colorectal tumor model.

2. Result and Discussion

2.1. Nanoparticle Preparation and Characterization

The DOX and miRNA-145 loaded, targeted MSN (Dm@TMSN) delivery system was stepwise engineered as illustrated in Figure 1. MSN was synthesized and modified with 3-mercaptopropyltrimethoxysilane (MPTMS) to introduce thiol groups on the surface. The surfactant template of cetrimonium bromide (CTAB) was then removed to produce the empty MSN with SH on the surface (MSN-SH). Sulfur was identified in energy-dispersive X-ray spectroscopy (EDS) of MSN-SH, indicating successful decoration of thiol groups on the nanoparticles (Figure S1, Supporting Information). Then, MSN-SH was modified with 2,2'-dipyridyldisulfide to introduce pyridyldithiol reactive groups on the nanoparticle surface (MSN-s-s-PD).^[20] The assay

for thiol groups on the nanoparticle surface using Ellman's reagent indicated that >96% of the thiol groups were transformed into the active pyridyldithiol forms (data not shown).

DOX was next loaded into the MSN-s-s-PD (D@MSN-s-s-PD), and then the nanoparticles were sequentially modified with PEI-SH (D@MSN-PEI) and then OPSS-PEG-WL8/OPSS-PEG (molar ratio 1:10) to generate DOX-loaded targeted MSN (D@TMSN) with 8.2% DOX loading. MiRNA-145 was complexed with the nanoparticle surface to finally produce Dm@TMSN. An electrophoretic mobility shift assay indicated that complete adsorption of miRNA-145 on the nanoparticles was obtained when the N/P ratio (the ratio of moles of the amine groups of cationic polymer to those of the phosphate ones of nucleic acid) was greater than 24 (Figure S2, Supporting Information). High-resolution transmission electron microscopy (HRTEM) showed that the nanoparticles had spherical morphology with a diameter of ≈ 100 nm (Figure 2A). The wormlike mesostructure with pore sizes of 2–3 nm observed from TEM images was clear for D@MSN-s-s-PD (Figure 2AI), but was obscure after PEI and PEG modification and miRNA-145 loading to form Dm@TMSN (Figure 2AII). The evolution of size and zeta potential during Dm@TMSN preparation reflected the sequential conjugation of PEI and PEG, and also the adsorption of miRNA on the nanoparticle surface (Figure 2B,C). The resulting Dm@TMSN had hydrodynamic size of 183 nm and zeta potential of 23.3 mV (Table S1, Supporting Information). The nanosystem had good colloidal stability in PBS with 10% FBS at 37 °C for at least 24 h (Figure 2D) and also in PBS at 4 °C for at least 30 d (Figure S3, Supporting Information). Based on electrophoresis, compared to fast degradation of naked miRNA-145 in 10% FBS, when bound to the nanoparticles, miRNA-145 resisted degradation (Figure 2E). Other nanoparticles carrying only one molecule (m@TMSN, D@TMSN), as well as the empty nanocarrier (TMSN) and nontargeted control (Dm@MSN), were also prepared. For comparison of DOX release under various physiological conditions, DOX-loaded MSN functionalized with both phosphonate and PEI (D@MSN-Phos/PEI) were also prepared according to the literature.^[4c,d,6] The sizes and zeta potentials of these nanoparticles were measured using a Zetasizer Nano ZS instrument and summarized in Table S1 (Supporting Information).

Efficient nanoparticle uptake in target cells is important for the cargoes (DOX and miRNA-145) to exert their activity, as both of their targets are located in different locations in the cells. We then evaluated the uptake of the nanocarrier in the model cell line SW480, which expresses high levels of GRP78 in the cell membrane (Figure S4, Supporting Information).^[19] The empty nontargeted MSN and targeted WL8-MSN were labeled with FITC as a fluorescent probe. As expected, WL8 peptide modification increased the nanoparticle uptake in SW480 cells by nearly threefold, conferring the active targeting capacity (Figure 2F,G). This targeting effect could be completely inhibited when preincubation with free WL8 peptide, suggesting that the improved uptake was resulted from the specific interaction between WL8 and GRP78 on the SW480 cell surface. The difference in uptake between TMSN and nontargeted MSN indicated not only the successful decoration of WL8 to the nanoparticles, but also the feasibility of WL8-mediated targeted delivery. We also identified, through immunohistochemical assay of the

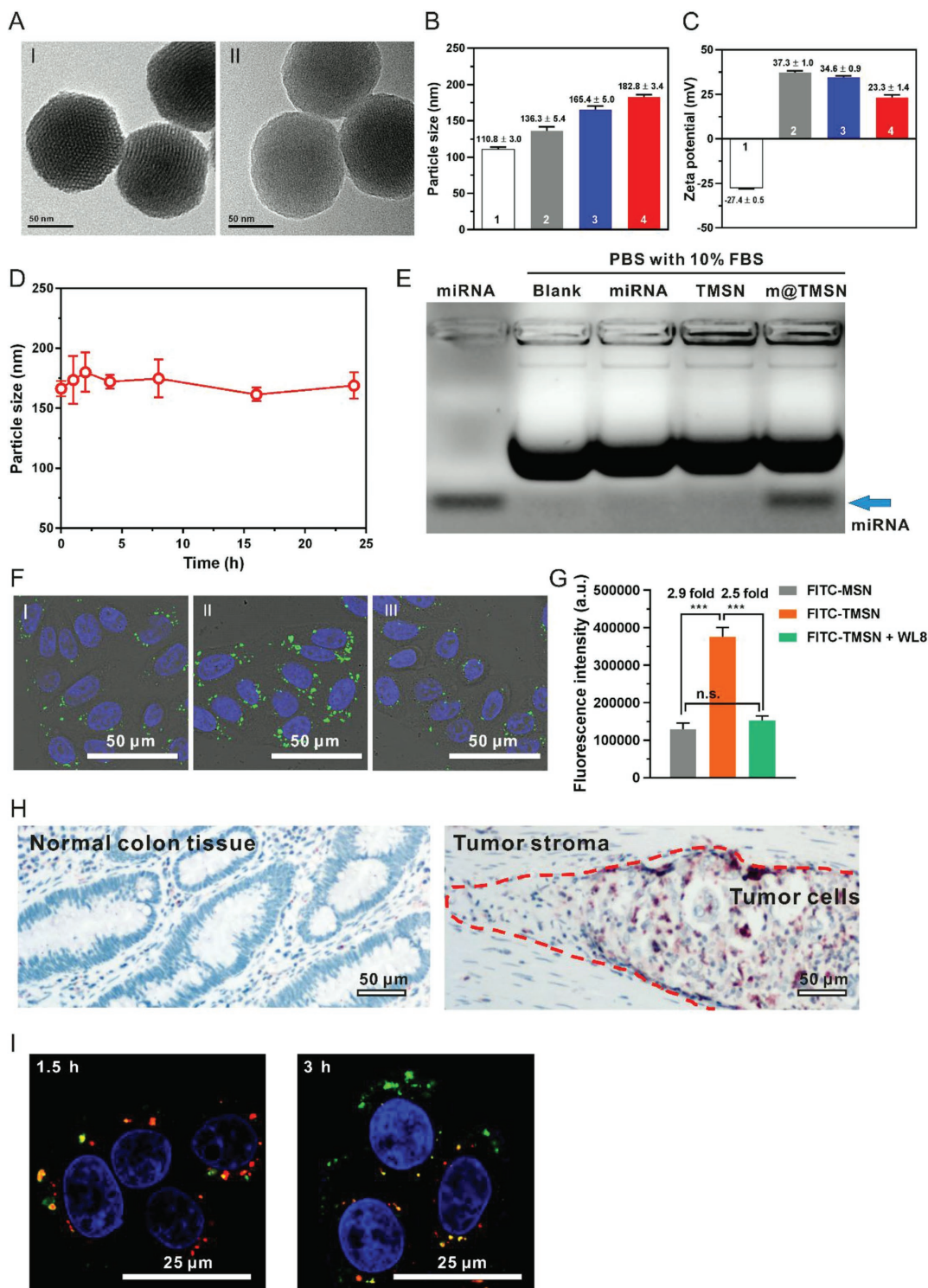


Figure 2. Characterization of Dm@TMSN. A) HRTEM image of D@MSN-s-s-PD (I) and Dm@TMSN (II). Evolution of B) particle size and C) zeta potential in the process of preparing Dm@TMSN. 1: D@MSN-s-s-PD; 2: D@MSN-PEI; 3: D@TMSN; 4: Dm@TMSN. D) Colloid stability of Dm@TMSN in PBS with 10% FBS after 24 h incubation at 37 °C. E) Protective effect of the nanocarrier (TMSN) on miRNA-145 in PBS with 10% FBS at 37 °C for 24 h detected by agarose gel electrophoresis. F) Cellular uptake in SW480 cells after 4 h incubation with FITC-labeled MSN (FITC-MSN) (I), TMSN (FITC-TMSN) (II), and FITC-TMSN plus free WL8 (III) at 37 °C was observed under CLSM (Ex: 488 nm, Em: 520 nm). G) Quantification of cellular uptake in panel (F). H) Representative immunohistochemical staining showing high GRP78 expression in colon cancer patient samples, compared to that in human normal colon tissues. I) Representative CLSM images of lysosomal escape of m@TMSN (miRNA-145 labeled with FAM) (green, Ex: 488 nm, Em: 520 nm) in SW480 cells. Lysosomes were stained with LysoTracker Red (red, Ex: 577 nm, Em: 590 nm). Data represent mean \pm s.d. for $n = 3$. *** $p < 0.001$.

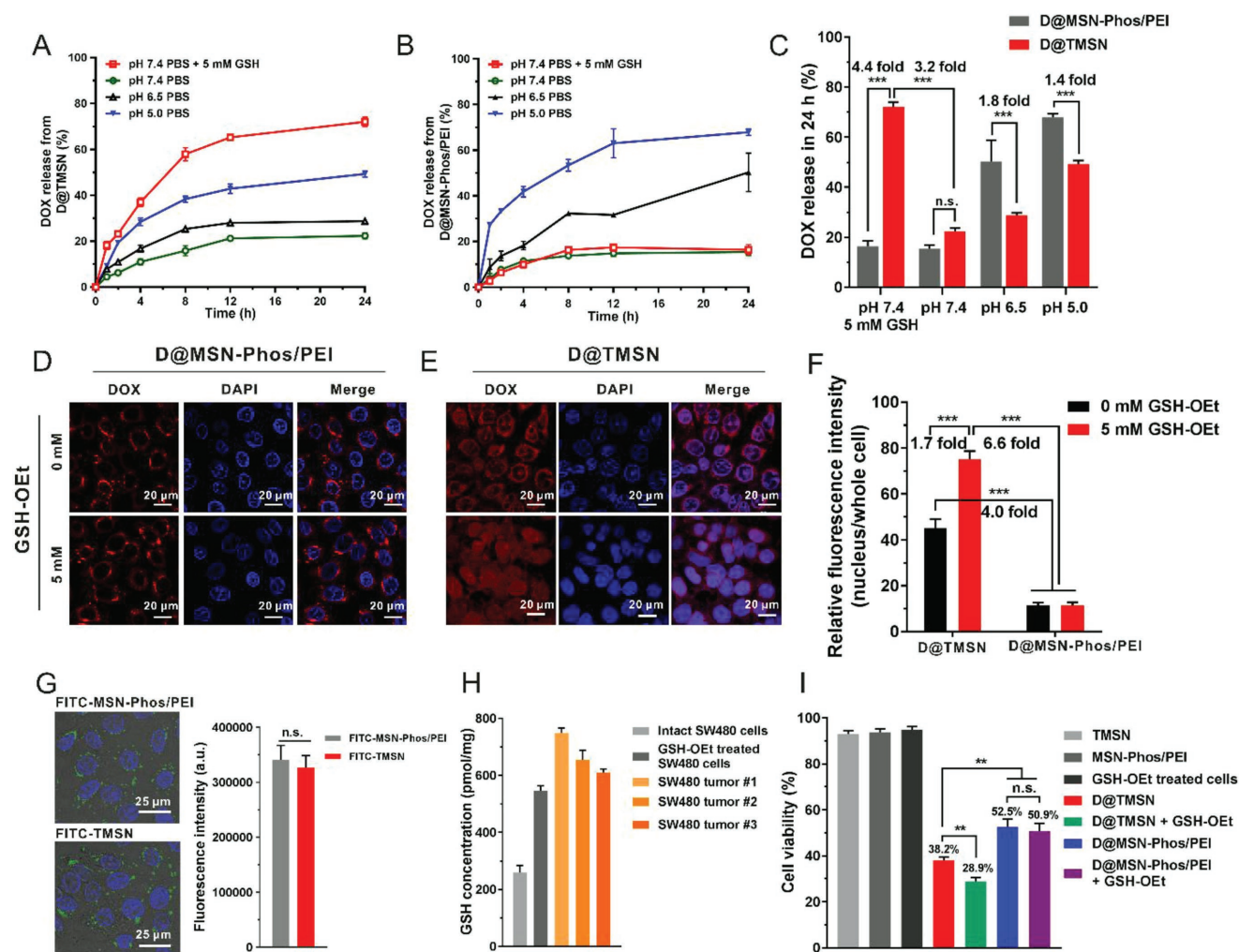


Figure 3. Redox-responsive enhanced DOX release, intranuclear distribution, and cytotoxicity of D@TMSN compared to D@MSN-Phos/PEI. Release profiles of DOX from A) D@TMSN and B) D@MSN-Phos/PEI in pH 5.0, pH 6.5, and pH 7.4 PBS with and without 5×10^{-3} M GSH. C) The DOX release in 24 h was statistically compared. SW480 cells were pretreated with or without 5×10^{-3} M GSH-OEt for 2 h and then incubated with D) D@MSN-Phos/PEI or E) D@TMSN for 4 h. CLSM images of the intracellular DOX distribution are shown. F) Quantitative assay of the DOX fluorescence intensity in the nucleus relative to the whole cells shown in panels (D) and (E) using the Image-Pro Plus 6.0 software. G) CLSM images and quantitative analysis of cellular uptake in SW480 cells after 4 h incubation with FITC-labeled TMSN and MSN-Phos/PEI. H) The GSH levels detected in the SW480 cells treated with or without 5×10^{-3} M GSH-OEt for 2 h and in three separate orthotopic SW480 tumors in mice. I) The viabilities of SW480 cells treated with D@TMSN and D@MSN-Phos/PEI were evaluated using CCK-8 assay. SW480 cells were pretreated with or without 5×10^{-3} M GSH-OEt for 2 h, and then incubated with the nanoparticles containing 3×10^{-6} M DOX for 4 h, then in fresh medium for 48 h. The mean \pm s.d. from three independent replicates is shown. $**p < 0.01$, $***p < 0.001$.

tissues from 28 colorectal cancer patients, that GRP78 expression in tumor cells was higher than that in the tumor stoma and adjacent normal tissues (Figure 2H and Figure S5, Supporting Information). These observations further confirmed that GRP78 receptor is a clinically relevant target that can be pursued for targeted drug delivery.

Efficient escape from lysosomes into the cytosol is required for nonviral nucleic acid delivery vehicles, which also prevents nucleic acid degradation by lysosomal nucleases.^[21] We investigated the lysosomal escape behavior of the nanocarrier, which is important for effective miRNA delivery. The trafficking of the m@TMSN in SW480 cells was monitored under CLSM (Figure 2I). At 1.5 h after incubation, green dots (FAM labeled miRNA-145)

colocalized (yellow) with the red LysoTracker-labeled lysosomes, indicating the trap of the miRNA-145-loaded nanocarrier in the lysosomes. At 3 h, part of the green dots separated from the red lysosomes, indicating lysosomal escape, which is known to be conferred by the PEI-mediated “proton sponge” effect.^[13]

2.2. Redox-Responsive Enhanced DOX Release of D@TMSN In Vitro

We then investigated the DOX release from D@TMSN under various physiological conditions with the previously reported DOX-loaded MSN-Phos/PEI (D@MSN-Phos/PEI)^[4c] as the control (Figure 3A–C). Both nanoparticles could effectively

restrain the DOX release in pH 7.4 PBS (below 25% release in 24 h), which can be helpful in hindering DOX leakage in circulation before they navigate to the tumor sites. Moreover, such slow release can greatly decrease the toxicity to the normal tissues, even when the nanoparticles are trapped there. In pH 6.5 PBS simulating the acidic tumor microenvironment,^[12] DOX release was significantly increased as for D@MSN-Phos/PEI. This result was consistent with the literature, indicating that the protonation of DOX effectively facilitated its release from the pores of MSN.^[4c] It is noted that such high release in pH 6.5 PBS as for D@MSN-Phos/PEI was 1.8-fold higher than that for D@TMSN. This observation indicates that D@TMSN could more efficiently hinder the premature DOX release in the tumor microenvironment before they can be internalized in the tumor cells. Such effect can be ascribed to the “woven” PEI covered on the surface of D@TMSN which acted as a gatekeeper to prevent DOX leaking from the pores.

In pH 5.0 PBS, which simulates the environment of acidic lysosomes, DOX release from D@MSN-Phos/PEI was 1.4-fold faster than from D@TMSN. However, such superiority would be lost after the rapid lysosomal escape of the nanoparticles and translocation into the neutral cytosol, where DOX release from D@MSN-Phos/PEI was substantially restrained and this would inhibit DOX cytotoxicity. In contrast, DOX release from D@TMSN in the simulated cytosol (pH 7.4 PBS with 5×10^{-3} M GSH) was enhanced, and reached 4.4-fold higher release level compared to that from D@MSN-Phos/PEI under the same condition. The $0.5\text{--}10 \times 10^{-3}$ M of GSH in tumor cells^[14a] can enhance hydrolysis of the disulfide bonds between the PEI and the nanoparticle surface, and finally remove the PEI gatekeeper (Figure S6, Supporting Information). This effect dramatically facilitated the release of the trapped DOX, as it showed that the presence of 5×10^{-3} M GSH led to 3.2-fold increased DOX release in 24 h as for D@TMSN. Such quick release kinetics can be beneficial to confer high intracellular DOX concentration and then exert the higher cytotoxicity, as the safe, rapid, and sufficient release of the drugs in the cells was the prerequisite for the active molecules to freely act on the target and effectively kill the tumor cells.^[10,22]

2.3. Redox-Responsive Enhanced DOX Intranuclear Distribution and Cytotoxicity of D@TMSN in SW480 Cells

We next investigated the toxicity of the two nanoformulations (D@TMSN and D@MSN-Phos/PEI) to the tumor cells (SW480). It is noted the diameter of nuclear pore complexes (NPCs) is only 20–70 nm,^[23] thus the two nanoformulations with their bigger sizes (≈ 100 nm under TEM) could not directly enter into the nucleus, where DOX can intercalate with DNA base pairs and induce DNA damage by mammalian DNA topoisomerase II.^[24] We thus hypothesize that the differential release kinetics of the two formulations will eventually influence their toxicity to the SW480 cells.

We first examine the intranuclear distribution of DOX using CLSM. It showed that low amount of DOX was detected in the nuclei of the cells treated with D@MSN-Phos/PEI (Figure 3D,F).

However, many bright red fluorescent spots only aggregated at the perinuclear space (Figure 3D), indicating that DOX was still trapped in the nanocarrier. This can be ascribed to extremely low DOX release in the neutral cytosol environment as shown in the *in vitro* test (Figure 3B). In contrast, much more DOX was released in the cells treated with D@TMSN and then translocated into the targeted site (nucleus), which led to nearly fourfold higher nucleus/whole cell fluorescence were observed for the cells treated with D@TMSN compared to that with D@MSN-Phos/PEI (Figure 3E,F). It should be noted that there was no difference between the uptake of the two nanocarriers by SW480 cells during the same period of time (4 h incubation with the nanoparticles) (Figure 3G). This comparable cell uptake can be ascribed to the high positive charge (47.9 mV) as for D@MSN-Phos/PEI and the relatively low charge (34.6 mV) but with the GRP78 targeting property as for D@TMSN (Table S1, Supporting Information). Thus, the differential intranuclear distribution can be ascribed to their distinct DOX release efficiency in the cells.

Elevated GSH levels in the cytosol make it a useful internal stimulus for induction of intracellular drug release from nanocarriers.^[25] To further confirm that enhanced intracellular DOX release and distribution in the nucleus as for D@TMSN were GSH dependent, as shown in the *in vitro* test (Figure 3A), cells were preincubated with monoethyl ester of GSH (GSH-OEt, 5×10^{-3} M) before treatment with the nanoformulations. GSH-OEt was used since the anionic nature of GSH impedes internalization into cells. As a neutral molecule, GSH-OEt can penetrate cellular membrane prior to being hydrolyzed by esterases to produce GSH, thus increasing the intracellular concentration of GSH.^[26] After pretreatment with GSH-OEt, the DOX nucleus/whole fluorescence as for the D@TMSN was further enhanced by 1.7-fold (Figure 3E,F). More importantly, nearly 80% DOX in the cells was uniformly distributed in the nucleus (Figure 3E,F), which is required for cytotoxicity. GSH-OEt did not influence the intracellular DOX distribution for D@MSN-Phos/PEI (Figure 3D,F).

Interestingly, although GSH-OEt pretreatment resulted in significantly increased GSH in the cells compared to that in the intact cells, such resulted GSH level was still lower than that observed in three separate orthotopic SW480 tumors (Figure 3H). This observation suggested that in the tumors *in vivo* the GSH-responsive DOX release and nucleus translocation as for D@TMSN may be at least comparative to what we observed *in vitro* or even faster.

We then evaluated if the improved intracellular DOX release and intranuclear distribution will result in enhanced cytotoxicity. As expected, D@TMSN led to dramatically enhanced toxicity to SW480 tumor cells compared to D@MSN-Phos/PEI (Figure 3I). The viability of the cells treated with D@TMSN was 30% lower than that treated with D@MSN-Phos/PEI. Moreover, the GSH-OEt preincubated cells, which more accurately reflected the *in vivo* situation, were more sensitive to D@TMSN. The cell viability was further decreased to only 28.9%, $\approx 45\%$ lower than that of the cells treated with D@MSN-Phos/PEI. However, the involvement of GSH-OEt did not alter the sensitivity of the cells to D@MSN-Phos/PEI. The empty TMSN, MSN-Phos/PEI, and GSH-OEt alone did not cause toxicity to the cells.

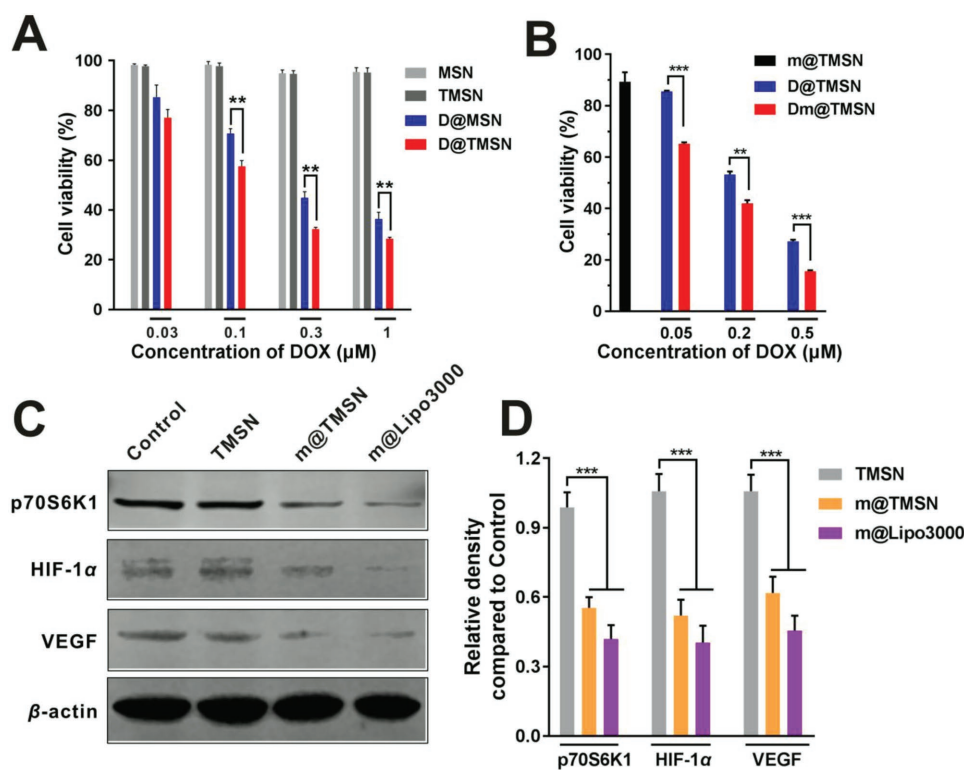


Figure 4. Cytotoxicity and expression of p70S6K1, HIF-1 α , and VEGF in SW480 cells. A) Cell viability of SW480 cells treated by D@TMSN and other control (empty MSN, empty TMSN, and nontargeted D@MSN). B) MiRNA-145 increased the sensitivity of SW480 cells to D@TMSN. C) The effect of miRNA-145-loaded TMSN (m@TMSN) on the expression of p70S6K1, HIF-1 α , and VEGF in SW480 cells. The miRNA-145-loaded Lipofectamine 3000 (m@Lipo3000) was used as the positive control. The cell alone was set as negative control. D) Quantitative analysis of relative protein expression. The data are presented as relative gray compared to control. All data represent means \pm s.d. for $n = 3$. ** $p < 0.01$, *** $p < 0.001$.

2.4. Cytotoxicity and Expression of p70S6K1, HIF-1 α , and VEGF Influenced by Dm@TMSN in SW480 Cells

Due to the superiority of improved DOX release, enhanced nuclear distribution, and increased cytotoxicity of D@TMSN compared to D@MSN-Phos/PEI, we thus chose D@TMSN to complex miRNA-145, generating Dm@TMSN for following combination efficacy. It showed that compared to nontargeted D@MSN, D@TMSN led to much higher toxicity to SW480 cells at DOX concentrations of 0.1– 1×10^{-6} M (Figure 4A). This effect may be attributed to the improved cell uptake mediated by the WL8 peptides (Figure 2F,G). Although miRNA-145 alone was nontoxic to the cells, it can synergistically enhance DOX toxicity to the cells (Figure 4B). The underlying mechanism may be related with the effect of miRNA-145 on suppressing the prosurvival protein (VEGF) (Figure 4C). It is known that besides binding to VEGFR in the tumor vascular endothelial cells for promoting angiogenesis, VEGF can also promote survival of tumor cells through directly interacting with the VEGFR2 receptor on the tumor cell surface.^[27] We confirmed VEGFR2 expression in the SW480 cells (Figure S7, Supporting Information).

The expression of p70S6K1 (the target of miRNA-145) and its two downstream functional proteins (HIF-1 α and VEGF) in the cells treated with m@TMSN was remarkably suppressed to ≈ 56 , 50, and 58% level of those treated with the empty TMSN, respectively (Figure 4C,D). This effect is also comparable with

that conferred by the miRNA-145-loaded Lipofectamine 3000 (m@Lipo3000). As for the in vivo situation, the suppression of HIF-1 α and VEGF is expected to exert strong antiangiogenic effect to inhibit tumor growth,^[16] which may earn superior synergistic antitumor efficacy with the combination of DOX.

2.5. Orthotopic SW480 Colorectal Tumor Targeting

We investigated if the WL8 modified nanoparticles can actively target the tumor in vivo. Orthotopic tumor models are considered to be more clinically relevant than ectopic ones, and thus are preferred in preclinical research.^[28] We established an orthotopic colorectal cancer model using SW480 cells, according to previous literature^[29] with moderate modification. SW480 cells mixed with matrigel were injected into the submucosa of the cecum wall. Trypan blue was used to confirm an accurate position for injection (Figure 5A1,2). Orthotopic tumor growth was confirmed by necropsy (Figure 5A3), pathological assay (Figure 5A4), and bioluminescence imaging (Figure 5A5). The pathological section showed the whole histological structure of cecum and clearly demonstrated the anatomical location of the orthotopic tumor, which was inside the submucosa as expected.

The accumulation of Cy5.5-labeled MSN and TMSN in the orthotopic tumor was detected using a multimodal luminescence and X-ray computed tomography imaging system (Figure 5B,C). The bioluminescence signal of the orthotopic SW480 tumor,

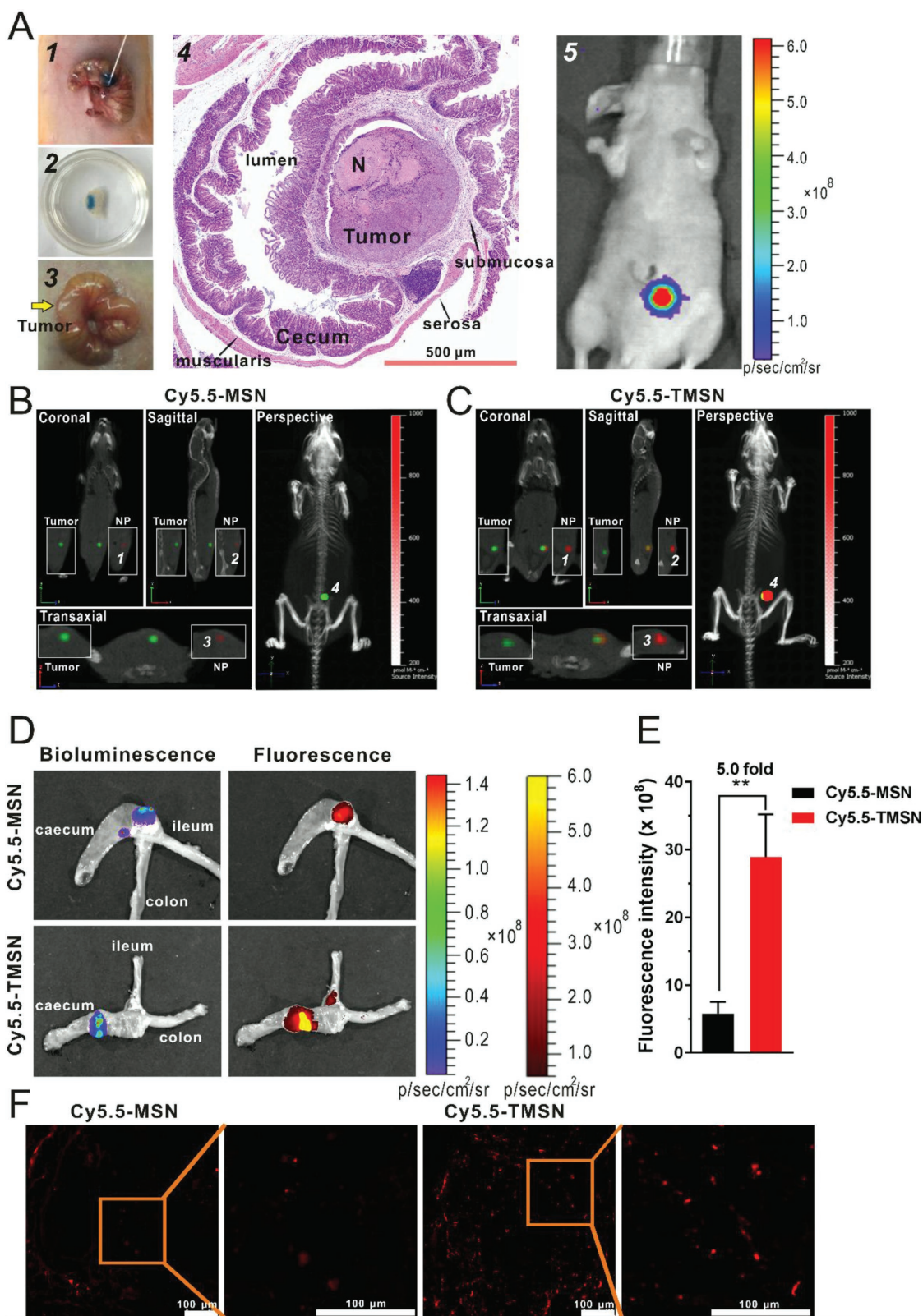


Figure 5. Establishment of an orthotopic colorectal cancer model in nude mice and in vivo tumor targeting of the nanoparticles. A) The technique of cecum wall injection and the confirmation of orthotopic colon cancer model. 1: Cecum wall injection technique was established by using trypan blue as the simulated cell suspension; 2: Excised cecum wall trypan blue staining was immersed in the PBS solution; 3: Macroscopic orthotopic tumor (denoted with yellow arrow) in the cecum by autopsy third week after tumor cell inoculation; 4: H&E staining showed the anatomical position of submucosa

fluorescence signal of the nanoparticles, and the skeleton structure of the mice were synchronously recorded and the tri-modal images were reconstructed to visualize the accumulation of nanoparticles in the tumors. It showed that 24 h after nanoparticle injection, low fluorescence appeared in the bioluminescent tumor sites in MSN group. However, much stronger colocalization of fluorescent nanoparticles and the bioluminescent tumors were observed in TMSN groups. This observation is confirmed from coronal, sagittal, transaxial, and the whole perspective angles, demonstrating the targeting contribution of WL8 peptides.

Ex vivo imaging of the excised cecum showed the similar results (Figure 5D,E). WL8 peptide modification on the nanoparticles (TMSN) led to nearly fivefold higher fluorescence intensity in the tumors of mice compared to that treated with nontargeted MSN. The distribution of nanoparticles in tumors was further examined by frozen section and observed under CLSM (Figure 5F). It was shown that compared to MSN, TMSN not only had a more accumulation at the tumor region but also enabled to penetrate more deeply into the interior of the tumor where GRP78 protein was reported to have a higher expression.^[30] All these observations indicated the WL8 peptide modification could confer the nanoparticles with the excellent property of targeted accumulation in orthotopic SW480 tumors.

Long circulation in blood is a prerequisite for successful in vivo tumor targeting. We also examined the circulation time of the WL8-modified targeted MSN (TMSN) using female SD rats as the animal model and Cy5.5 as the fluorescent probe (Cy5.5-TMSN) for quantification. It showed that TMSN displayed a relatively long half-life of ≈ 8.0 h (Figure S8, Supporting Information). This may be partially ascribed to the modified PEG which can confer good colloidal stability shown in even serum-contained medium (Figure 2D).

2.6. Antitumor and Antimetastasis Efficacy in Orthotopic SW480 Colorectal Tumor Model

Based on the preferential targeting accumulation and penetration of the nanocarrier in tumors, we then further investigated the in vivo antitumor activity of Dm@TMSN using the established orthotopic colon cancer model. The evaluation program was carried out according to the schedule in Figure 6A. 12 d after orthotopic tumor implantation, mice were divided into six groups according to bioluminescence intensity and intravenously injected with various formulations every 3 d with five repetitions (day 0, 3, 6, 9, 12). Bioluminescence imaging was used to monitor tumor growth every week (day 7, 15, 22, 29, 36), and representative bioluminescence images of the mice in each group are presented in Figure 6B. The bioluminescence intensity was well proportional to the number of the tumor

cells (Figure S9, Supporting Information), thus this method made it feasible to continuously and noninvasively monitor the tumor growth conveniently.

Same to the effect of saline, empty nanocarrier (TMSN) could not delay the tumor growth (Figure 6C). It is noted that the targeted single-drug loaded nanoparticles (m@TMSN and D@TMSN) and nontargeted codelivery nanoparticles (Dm@MSN) already exhibited dramatic effect of inhibiting tumor growth (Figure 6C). However, the tumors regressed in the mice treated with Dm@TMSN, showing the strongest antitumor effect (Figure 6C). At the end of the experiment (day 38), the mice were sacrificed and tumors were excised for weighting. The tumor weights of mice treated with Dm@TMSN were 3–7.5-fold lighter than those treated with other controls (Figure 6D).

During the therapy, the mice body weight from all groups had a similar increase, suggesting no overt toxicity (Figure 6E). Moreover, hematoxylin and eosin (H&E) staining of major organ including heart, liver, spleen, lung, and kidney in all groups showed no obvious histological toxicity compared with the control group, showing the nanoparticles were well-tolerated and biocompatible at the doses used (Figure S10, Supporting Information).

Metastases are the leading cause of death for colorectal cancer patients.^[31] Up to 60% of colorectal cancer patients have metastases in the liver, and up to 35% of the metastases occur exclusively in this organ.^[32] The orthotopic colon cancer model established in this study could spontaneously form organ metastases. Thus, at the end of the test (day 38), major organs (liver, intestine, lung, and spleen) and mesenteric draining lymph nodes (LN) from all the mice were excised for antimetastasis evaluation using bioluminescence imaging (Figure 7). The bioluminescence imaging was sensitive, as it can detect as little as 100 tumor cells in vitro (Figure S9, Supporting Information), thus tiny metastasis which cannot be tracked by naked eye or conventional histopathological method can also be captured.

For the saline group, all the mice had extensive metastases in the intestine and mesenteric draining LN. More than half of the mice had lung and liver metastases, and one-third of the mice also exhibited small spleen metastases (<2 mm). The mice in the TMSN group had similar metastasis pattern to that of the saline group. In sharp contrast, metastases were significantly inhibited with the treatment of miRNA-145-involved targeted nanoformulations (m@TMSN and Dm@TMSN), and no detectable metastases were found in the liver, lung, and spleen. As for the other two groups (D@TMSN, Dm@MSN), the antimetastasis effect was relatively weak. It is noted that reduced tumor burden may also contribute to the enhanced antimetastatic effect, which can be seen from the comparison between the effects of empty TMSN and D@TMSN (Figure 7). However,

of the orthotopic tumor; 5: In vivo bioluminescence imaging of the orthotopic colon tumor in nude mice fourth week after tumor cell inoculation. B,C) 24 h after i.v. injection of the Cy5.5 labeled MSN (Cy5.5-MSN) and TMSN (Cy5.5-TMSN), respectively, the tumor targeting was observed using the IVIS Spectrum CT multimodal imaging system. The red fluorescence signals denoted the Cy5.5-labeled nanoparticles (NP), and the green signals indicated the orthotopic tumor on the cecum wall. The nanoparticle distribution in the tumors observed from the coronal (1), sagittal (2), transaxial (3), and the perspective (4) directions were separately shown. D) Representative ex vivo bioluminescence (left) and fluorescence (right) imaging of the orthotopic tumor in the cecum 24 h after i.v. injection of the Cy5.5-TMSN and Cy5.5-MSN. E) Quantified fluorescence intensity in the orthotopic tumors in panel (D). F) CLSM image of the frozen sections of the tumors in panel (D). Data represent mean \pm s.d. for $n = 3$. $**p < 0.01$.

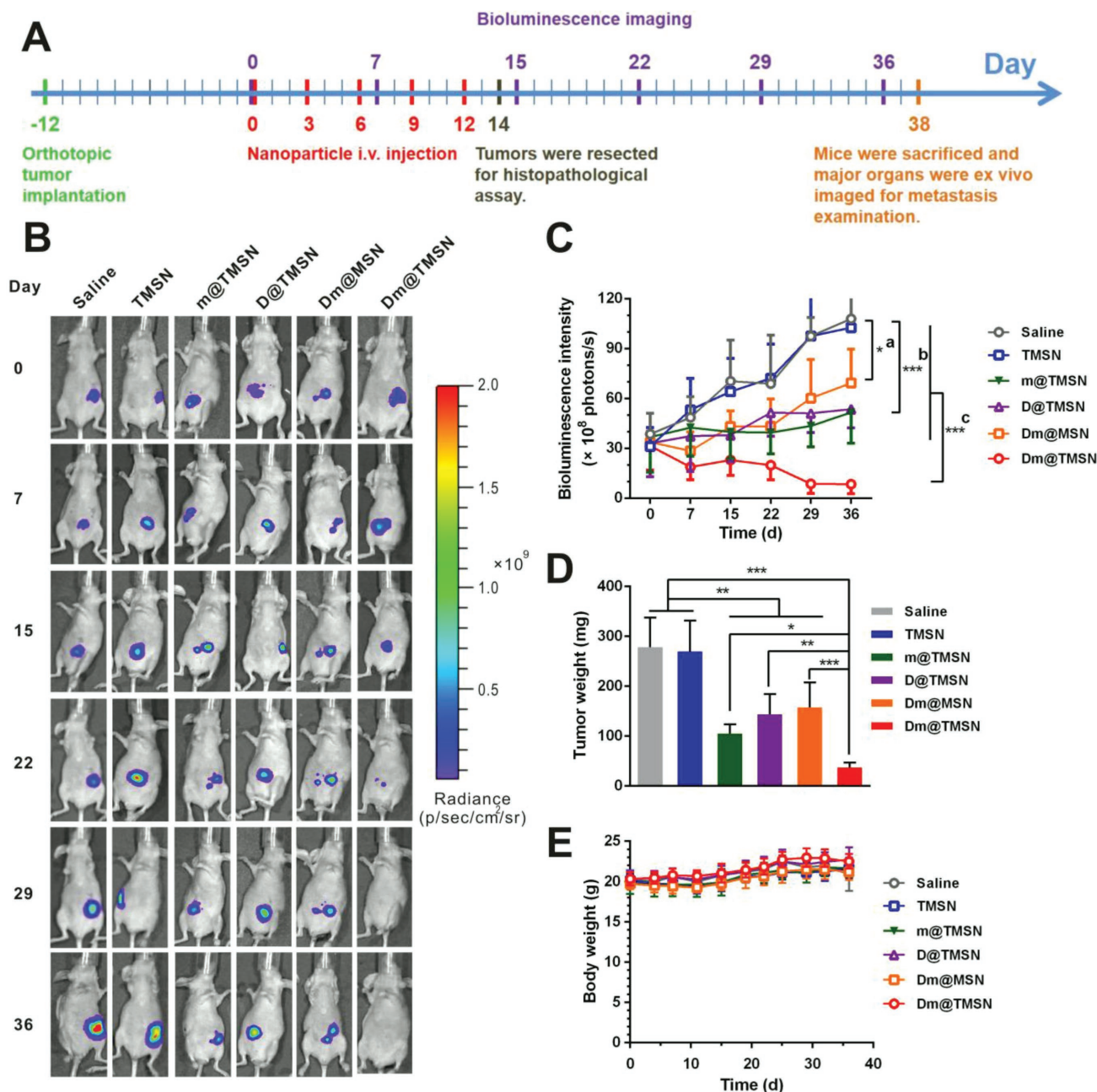


Figure 6. In vivo combination therapy using Dm@TMSN in mice bearing orthotopic colorectal tumors. A) Treatment regimen. B) Representative in vivo bioluminescence imaging of the orthotopic colorectal tumor at the indicated time. C) Tumor growth profiles obtained through quantifying the bioluminescence in panel (B). (a): Dm@MSN versus saline or empty TMSN. (b) m@TMSN and D@TMSN versus saline or empty TMSN. (c) Dm@TMSN versus all other groups. D) Tumor weight on the last day (day 38) of the test. E) Mice body weight. The data are expressed as mean ± s.d. ($n = 5-6$). * $p < 0.05$, ** $p < 0.01$, *** $p < 0.001$.

even the tumors treated with m@TMSN and D@TMSN had comparable decreased volumes, the resulted metastasis patterns were still significantly different. In contrast to 40% metastatic frequency occurred in liver, lung, and spleen of the mice treated with D@TMSN, no detectable metastases were observed in these organs of the mice treated with m@TMSN (Figure 7). This observation indicates the specific antimetastatic effect of miRNA-145. We also performed pathological sections to further

confirm the metastases in the organs (Figure S11, Supporting Information). It should be noted that the sizes of some metastases were so tiny (<1–2 mm) in the liver, lung, and spleen that they were not easily to be checked through the routine section examination.

The enhanced antimetastasis effect observed in the miRNA-145-contained nanoparticles may be ascribed to the role of miRNA-145 in targeting p70S6K1 and thereafter

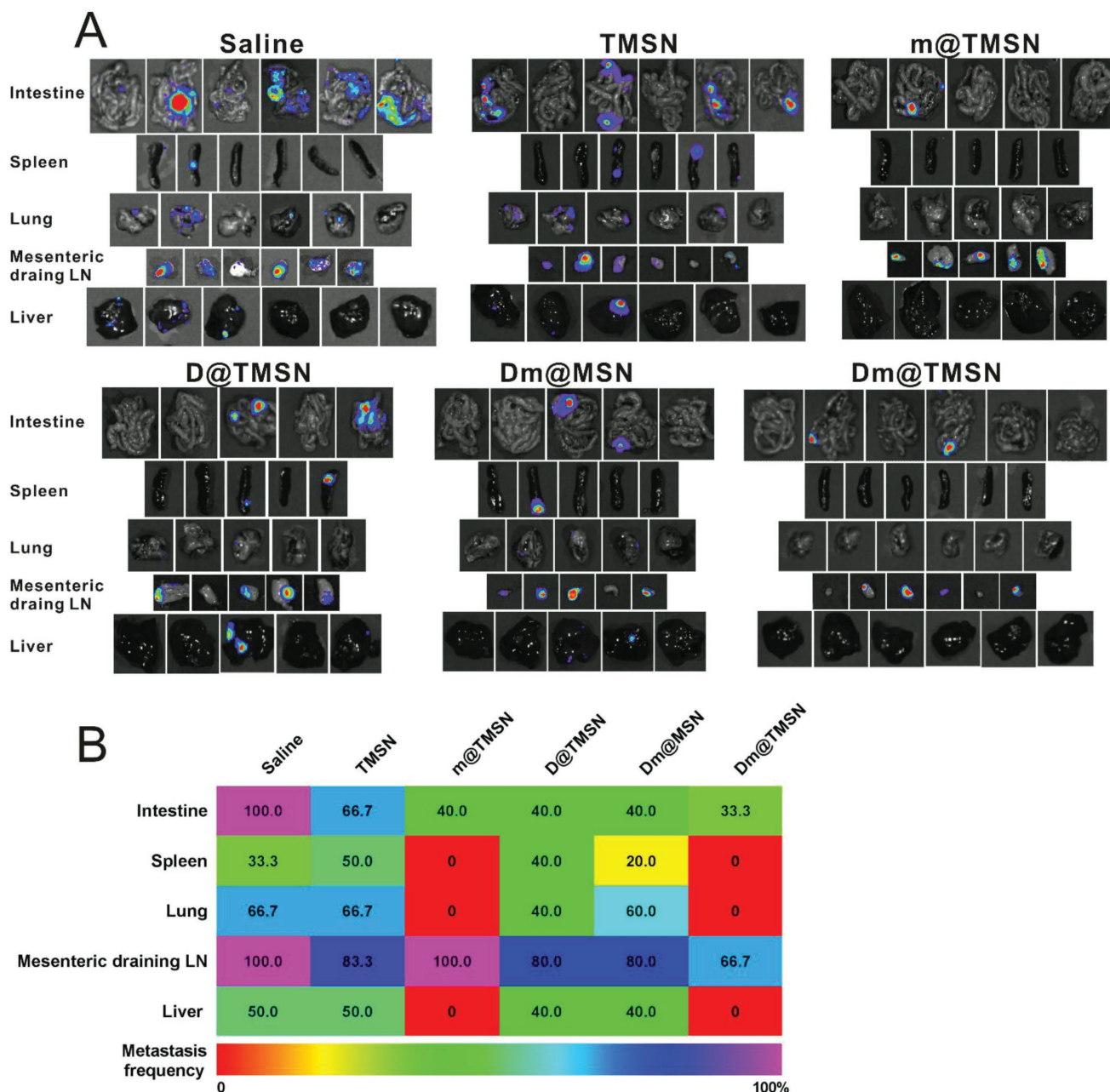


Figure 7. Dm@TMSN reduced metastatic spread of SW480 tumor cells to other main organs and tissues in the orthotopic colorectal tumor bearing mice. A) On the last day (day 38) of the animal study, ex vivo bioluminescence imaging was performed to examine the micro-metastasis in the main organs and tissues (intestine, spleen, lung, mesenteric draining LN, and liver). B) A heat map summarizes metastatic frequency of different treatments.

suppressing the expression HIF-1 α and VEGF^[16] (Figure 4C,D). These two proteins have been shown to be related to tumor angiogenesis and metastasis through diverse mechanisms.^[33] Immunohistochemistry assay revealed that the expressions of p70S6K1, HIF-1 α , and VEGF in tumor tissues were obviously suppressed by miRNA-145 delivered by TMSN (m@TMSN) or codelivered with DOX by TMSN (Dm@TMSN) (Figures S12–S14, Supporting Information). Empty TMSN had no silencing effect on these proteins expression. Moreover, immunohistochemistry showed m@TMSN

distinctly decreased the number of CD31 positive microvessel density (MVD) (Figure S15, Supporting Information), demonstrating the antiangiogenic effect of miRNA-145, which was closely correlated with suppressed organ metastases. With the effect of DOX, Dm@TMSN resulted in the least MVD compared to all the other control groups. All these results indicated that miRNA-145 could in vivo inhibit VEGF and HIF-1 α expression via p70S6K1 suppression, which was helpful for the synergistic antitumor and antimetastasis of the targeted co-delivery system.

3. Conclusion

To the best of our knowledge, this is the first study focusing on addressing the counterproductive interactions generated from intracellular, compartment-dependent delivery and release of two distinct therapeutic molecules. To overcome the challenge of properly codelivering DOX and nucleic acids to the proper intracellular location, we developed a new methodology of “weaving” PEI on the MSN surface through disulfide bonds to seal DOX in the MSN pores and serve as an electrostatic anchor for miRNA-145 complexing. This codelivery system could not only prevent drug preleakage before its navigation to tumor sites but also it achieved efficient release with the help of intrinsic redox stimulus in tumor cells. Moreover, WL8 peptide PEGylation to the nanoparticles conferred enhanced internalization in tumor cells and nanoparticle distribution in orthotopic colorectal tumors. By integrating the controlled release profiles and targeted delivery, this codelivery system realized synergistic antitumor efficacy *in vitro* and *in vivo*, and significant antimetastatic activity in an orthotopic colorectal tumor model. In conclusion, the smart delivery platform approach holds promise for codelivery of chemotherapeutics and nucleic acids for improved and synergistic anticancer therapy against primary tumors and metastatic disease.

4. Experimental Section

Materials, Cell Culture, and Animals: Tetraethylorthosilicate (TEOS, 98%), cetrimonium bromide (CTAB, 98%), 3-(mercaptopropyl)-trimethoxysilane (MPTMS), 2,2'-dipyridyldisulfide, glutathione (GSH), glutathione reduced ethyl ester (GSH-OEt), 4',6-diamidino-2-phenylindole dihydrochloride (DAPI), and fluorescein isothiocyanate (FITC) were purchased from Sigma-Aldrich (St. Louis, MO). Hydrofluoric acid and ethyl acetate were purchased from Sinopharm Chemical Reagent Co. Ltd. (Shanghai, China). PEI (1.8 kDa), fluorescamine, 3-mercaptopropionic acid (3-MPA), N-(3-dimethylaminopropyl)-3-ethylcarbodiimide hydrochloride (EDC), and N-hydroxysuccinimide (NHS) were obtained from Aladdin Chemistry Co. Ltd. (Shanghai, China). WL8 peptide (WIFPWQL) was synthesized by GL Biochem (Shanghai, China). Cy5.5 NHS ester was purchased from Lumiprobe (Hannover, Germany). OPSS-PEG-NHS (MW 5000) and OPSS-PEG (MW 5000) were purchased from JenKem Technology Co., Ltd. (Beijing, China). Doxorubicin hydrochloride was purchased from Beijing Hvsf United Chemical Materials Co., Ltd. (Beijing, China). Hsa-miRNA-145 mimics (miRNA-145, 5'-GUCCAGUUUCCAGGAAUCCU-3') and FAM-labeled miRNA-145 were purchased from RiboBio Company (Guangzhou, China). Dulbecco's modified Eagle's medium (DMEM), fetal bovine serum (FBS), PBS solution, penicillin, and streptomycin were gained from Thermo Fisher Scientific Inc. (Waltham, MA). Double distilled water was purified using a millipore simplicity system (Millipore, Bedford, MA). All other chemicals were of analytical grade and used without further purification.

SW480 human colorectal adenocarcinoma cell line was obtained from the ATCC (Manassas, VA). SW480 cell transfected with luciferase (SW480-luc) were constructed by Shanghai Model Organisms Center (Shanghai, China). Cells were cultured in DMEM medium with 10% FBS, 10^5 U L⁻¹ penicillin, and 100 mg L⁻¹ streptomycin. The culture was maintained at 37 °C in a humidified atmosphere containing 5% CO₂.

Female BALB/c nude mice (≈20 g) were provided by Shanghai Laboratory Animal Center (Chinese Academy of Sciences, Shanghai, China). The animal experiment designed in this study was approved by the ethical committee of Shanghai Jiao Tong University School of Medicine (SJTU-SM).

Preparation and Characterization of DOX and miRNA-145 Codelivery WL8-Modified Targeted MSN (Dm@TMSN): The MSN synthesis was performed according to ref. [34]. Briefly, 0.5 g CTAB was dissolved in 250 mL deionized water in a 500 mL flask. Then, 1.75 mL NaOH (2 M) was added as base catalyzer for sol-gel reaction. The mixture was then heated to 70 °C under a vigorous stirring, followed by the addition of 2.5 mL TEOS. After 1 min, 2.5 mL ethyl acetate was added, and the mixture was rapidly stirred for 30 s. Then, the reaction was allowed to age for 2 h. The MSN precipitation was collected by centrifugation (11 000 rpm, 10 min, Eppendorf AG 5810R, Germany), washed with methanol for three times and dried under vacuum overnight.

The surface of above CTAB-containing MSN was then functionalized with thiol groups. 500 mg of MSN were dispersed in 50 mL methanol by sonication, and 0.5 mL MPTMS was dropwise added to the solution. Then the mixture solution was refluxed at 80 °C under argon for 24 h. MSN-SH nanoparticles were collected by centrifugation (11 000 rpm, 10 min), washed with methanol for three times. The pore-generating template, CTAB, was removed via ion-exchange method under argon.^[35]

For the synthesis of pyridylthiol-terminated nanoparticles (MSN-s-s-PD), 250 mg of MSN-SH was dispersed in 25 mL methanol, and then was dropwise added into a 10 mL methanol solution containing 0.55 g 2,2'-dipyridyldisulfide and 0.2 mL glacial acetic acid. The mixture was stirred in the dark at room temperature for 24 h. The resulting nanoparticles (MSN-s-s-PD) were obtained by centrifugation (11 000 rpm, 10 min), and washed with methanol for three times. The thiol groups on the surface of MSN-SH and MSN-s-s-PD were quantified using Ellman's reagent.^[36]

To load DOX into the pore of MSN nanoparticles (D@MSN-s-s-PD), 50 mg of MSN-s-s-PD was mixed with 5 mL DOX solution (5 mg mL⁻¹) in PBS and sonicated for 5 min to obtain a well-dispersed suspension. After stirring at room temperature in the dark for 24 h, the suspension was centrifuged (11 000 rpm, 10 min), washed thoroughly with PBS until supernatant was colorless, and redispersed in 10×10^{-3} M HEPES buffer (pH 8.5). The loading efficiency of DOX into nanoparticles was measured by fluorescence method.^[20] 1.5 mg of D@MSN-s-s-PD was dissolved in 600 μL hydrofluoric acid and then diluted with 2.4 mL water. 8 mL water was added to 1 mL of the above solution, and the solution was analyzed by spectrofluorophotometer (Thermo Varioskan Flash, Waltham) using a standard calibration curve of DOX experimentally obtained (Ex, 488 nm; Em, 590 nm).

To weave the PEI (1.8 kDa) on the nanoparticle surface and seal the pore, PEI was sulfhydrylated as described^[37] and added into the D@MSN-s-s-PD solution and stirred for 3 h in the dark. For endowing targeting ability to the nanoparticles, WL8 peptides were linked to the OPSS-PEG-NHS to generate OPSS-PEG-WL8 according to the literature,^[38] and then mixed with OPSS-PEG at 1:10 molar ratio, and then dropwise added into the solution for 3 h reaction at room temperature. The resulting product (D@TMSN) was centrifuged (11 000 rpm, 10 min) and purified with deionized water. miRNA-145 was then complexed with D@TMSN to generate Dm@TMSN.

Other nanoparticles carrying only one molecule (m@TMSN, D@TMSN), as well as the empty nanocarrier (TMSN) and nontargeted control (Dm@MSN), were also prepared when the corresponding molecules were included during the preparation. For comparison of DOX release under various physiological conditions, DOX-loaded MSN functionalized with both phosphonate and PEI (D@MSN-Phos/PEI) were also prepared according to the literature.^[4c] FITC-labeled nanoparticles were generated by the chemistry of FITC with the PEI modified on the particles.

TEM images and EDS data acquisition were performed on an FEI Talos F200X system. The hydrodynamic size and zeta potential of nanoparticles were determined through dynamic light scattering (DLS) method and measured by ZetaSizer Nano ZS instrument (Malvern, Worcestershire, UK).

In Vitro Cellular Uptake: SW480 cells (5×10^4) were seeded onto coverslip in 24-well plate. When the cells reached about 80% confluence, the culture medium containing FITC-labeled MSN (FITC-MSN), TMSN (FITC-TMSN), and MSN-Phos/PEI (FITC-MSN-Phos/PEI) at FITC

concentration of $0.1 \mu\text{g mL}^{-1}$ was applied to the cells and incubated for 4 h, respectively. For WL8 peptide competition experiments, the cells were cultured with WL8 peptide (50-fold excess) for 2 h prior to addition of FITC-TMSN. The internalization images of nanoparticles were gained by using LSCM and the quantitation of fluorescence intensity in cells was analyzed by ArrayScan XTI High Content Analysis Reader (Thermo Fisher Scientific Cellomics, USA).

Lysosomal Escape: To perform intracellular tracking, SW480 cells (5×10^4) were seeded onto the coverslip glass in 24-well plate. After cells reached to 50–70% confluence, the growth medium was substituted for fresh medium containing m@TMSN (miRNA-145 labeled with FAM, $100 \times 10^{-9} \text{ M}$) (Ex 488 nm, Em 520 nm) and incubated for 0.5 h, then discarded the medium and continuously incubated with fresh medium for additional 1 and 2.5 h at 37°C . LysoTracker Red DND-99 (Ex 577 nm, Em 590 nm) (Invitrogen, USA) was used to stain the lysosomes according to the manufacturer's instructions. Then, the cells were washed three times with PBS, stabilized with 4% paraformaldehyde for 15 min. DAPI was used to stain nuclei. All intracellular trafficking images were characterized by CLSM (Leica SP8)

Redox-Responsive Drug Release in Vitro: To investigate the GSH-triggered DOX release, D@TMSN was dispersed in PBS (pH 7.4, 6.5, and 5.0) with or without GSH ($5 \times 10^{-3} \text{ M}$) in the centrifuge tubes. The tubes were placed in the gas bath at 37°C shaking at 120 rpm. At predetermined time intervals, the tubes were applied for centrifugation (11 000 rpm, 10 min) to pellet the nanoparticles. The concentration of DOX released in the supernatant was quantified by Shimadzu LC-20AT chromatographic system (Shimadzu, Kyoto, Japan), the excitation and emission wavelength were 488 nm and 590 nm. D@MSN-Phos/PEI were set as control.

To measure PEI release from nanoparticles, the empty TMSN were dissolved in PBS (pH 7.4) with or without GSH ($5 \times 10^{-3} \text{ M}$) in the centrifuge tubes. The tubes were shaken at 120 rpm at 37°C . At certain time intervals, tubes were taken out to measure PEI content in the supernatant by fluorescamine assay.^[39] Fluorescamine can react with primary amines in PEI to form pyrrolinones, which is excited at 406 nm and has emission peak at 476 nm.

Intracellular Redox-Responsive DOX Distribution: SW480 cells (5×10^4) were seeded onto the coverslip glass in 24-well plate, cultured for 24 h, and then treated with $5 \times 10^{-3} \text{ M}$ GSH-OEt for 2 h. Cells were washed with PBS and incubated with D@TMSN or D@MSN-Phos/PEI (containing $3 \times 10^{-6} \text{ M}$ DOX) for 4 h. The culture medium was then substituted by fresh medium for additional 20 h incubation. Then, the cells were fixed with 4% paraformaldehyde for 15 min at room temperature. After the nuclei staining with DAPI, the slides were washed with PBS three times, mounted and observed by CLSM (Ex 488 nm, Em 590 nm). Cells without GSH-OEt treatment were used as the control.

GSH Content Assay: Intact SW480 cells, SW480 cells pretreated with $5 \times 10^{-3} \text{ M}$ GSH-OEt for 2 h and orthotopic SW480 tumors were sampled and weighted, followed by measuring their GSH content by using GSH and GSSG Assay Kit according to the manufacturer's instructions (Beyotime, Shanghai, China). The result was represented as picomole of GSH per milligram of cells or tumor tissues.

Cell Viability: SW480 cells were seeded in the 96-well plates at a density of 8000 cells/well. After 24 h culture, the medium in the wells was replaced with fresh medium containing D@MSN, D@TMSN at DOX dose of 0.03, 0.1, 0.3, and $1 \times 10^{-6} \text{ M}$, respectively. After 48 h incubation, cells viabilities were determined using Cell Counting Kit-8 (Dojindo, Laboratories, Kumamoto, Japan) according to the manufacturer's instructions. The empty MSN and TMSN with the same concentrations were set as control. For the evaluation of combined cytotoxicity, m@TMSN (miRNA-145 $100 \times 10^{-9} \text{ M}$), D@TMSN (DOX at 0.05, 0.2, $0.5 \times 10^{-6} \text{ M}$), and Dm@TMSN containing miRNA-145 ($100 \times 10^{-9} \text{ M}$) and DOX (0.05, 0.2, $0.5 \times 10^{-6} \text{ M}$) were tested using the same protocol.

In a separate study, SW480 cells were pretreated with $5 \times 10^{-9} \text{ M}$ GSH-OEt for 2 h, then incubated with D@TMSN or D@MSN-Phos/PEI containing $3 \times 10^{-6} \text{ M}$ DOX for 4 h, and then the mediums were substituted with fresh medium for additional 48 h to investigate the influence of intracellular GSH on the nanoparticle-induced cytotoxicity.

Western Blotting: After SW480 cells were treated with TMSN, m@TMSN, and m@Lip3000 at miRNA-145 dose of $100 \times 10^{-9} \text{ M}$ for 48 h, the cells were lysed in RIPA buffer supplemented with PMSF (Beyotime, Shanghai, China) and PhosSTOP Phosphatase Inhibitor Cocktail (Roche, Rotkreuz, Switzerland). Total proteins were collected by centrifugation and quantified by BCA Protein Assay Kit (Thermo Scientific, Rockford, IL). $40 \mu\text{g}$ of proteins were separated by SDS-polyacrylamide gel, transferred to PVDF membranes (Millipore, Billerica, MA), and probed with specific antibodies (p70S6K1, HIF-1 α , and VEGF) followed by exposure to horseradish peroxidase-conjugated goat antirabbit antibody (Cell Signaling Technology, Danvers, MA).

Blood Clearance Kinetics: Female SD rats (170–180 g, $n = 5$) were intravenously injected via tail vein with Cy5.5-labeled targeted (Cy5.5-TMSN) and nontargeted nanoparticles (Cy5.5-MSN) at nanoparticle dose of 20 mg kg^{-1} . At appointed time points (10 min, 30 min, 1 h, 2 h, 4 h, 8 h, 12 h, and 24 h) postinjection, $200 \mu\text{L}$ of blood was sampled from orbital vein for quantification of the fluorescent signal (Ex 675 nm; Em 720 nm) as the method described in the literature.^[40] The nanoparticle content in blood was determined using the established standard curve between the Cy5.5 fluorescence intensity and the corresponding nanoparticle content. The nanoparticle content versus time plot was then obtained and the blood half-life of the nanoparticles was calculated using the WinNonlin software (Version 6.1 Pharsight, Mountain View, CA) according to noncompartmental model.

Orthotopic Colorectal Cancer Animal Model: The orthotopic colorectal cancer model was developed based on the literature.^[29] Female BALB/c nude mice (4–5 weeks old) were anesthetized by an intraperitoneal injection of ketamine-xylazine solution. The abdomen was sterilized with alcohol swabs. A median incision was then made through the lower ventral abdominal, and the cecum was exteriorized. A suspension of 2×10^6 SW480-luc cells in $50 \mu\text{L}$ serum-free DMEM medium containing $10 \mu\text{g mL}^{-1}$ matrigel was injected into the cecal wall using 30 G needle (Hamilton Company, Reno, NV). To prevent leakage, a cotton swab was held cautiously for 1 min over the site of injection. The cecum was then returned to the peritoneal cavity, the peritoneum and skin were closed with 5-0 suture, respectively. The tumor formation and growth were monitored using the Xenogen IVIS 200 imaging system (Caliper Life Sciences, MA).

Orthotopic Tumor Targeting of Nanoparticles: For tracking nanoparticle distribution in orthotopic colorectal tumor, targeted TMSN and nontargeted MSN were labeled with the near-infrared fluorophore Cy5.5. Briefly, 15 mg nanoparticles was dispersed in 4 mL carbonate buffer solution (pH 8.5), followed by addition of $200 \mu\text{L}$ of DMSO Cy5.5-NHS solution (1 mg mL^{-1}). The mixture was stirred at room temperature in the dark for 4 h, and the resulting products (Cy5.5-TMSN and Cy5.5-MSN) were obtained by centrifugation (11 000 rpm, 10 min), purified with deionized water washing.

15 d after of orthotopic tumor implantation, the tumor-bearing mice ($n = 3$) were injected through the caudal vein with Cy5.5-TMSN and Cy5.5-MSN at a Cy5.5 dose of 0.5 mg kg^{-1} , respectively. After 24 h, the mice were intraperitoneally injected with D-luciferin (150 mg kg^{-1} , J&K Chemical, Ltd., China). 8 min later, the mice were anesthetized and imaged under the IVIS Spectrum/CT imaging system (PerkinElmer, USA) to monitor bioluminescence and fluorescence signal (Ex 685 nm, Em 710 nm). Following the in vivo imaging, the mice were sacrificed and the cecum was exteriorized for ex vivo imaging. For further determining intratumoral distribution of nanoparticles, the tumor was frozen sliced for immunofluorescence by CLSM (Ex 633 nm, Em 710 nm).

Antitumor Therapy in Orthotopic Colorectal Tumor Model: 12 d after orthotopic tumor cell inoculation, the tumor-bearing mice were treated with saline (control), empty TMSN, m@TMSN, D@TMSN, Dm@MSN, and Dm@TMSN at DOX dose of 3 mg kg^{-1} and miRNA-145 dose of 75 nmol kg^{-1} on days 0, 3, 6, 9, and 12, respectively. Each groups included 5–6 mice. The tumor burden was monitored weekly using bioluminescence imaging and the body weight was recorded throughout the study. At the end of the study, the mice was sacrificed, the tumors were removed and weighted. Other major organs included intestine, liver, lung, spleen, and mesenteric draining LN were harvested for ex

vivo bioluminescent imaging and H&E histological assay to examine the metastasis.

In a separate study, on day 14 (2 d after the last injection of the nanoparticles), three mice from each group were sacrificed. The tumors were applied for H&E staining and immunohistochemistry assay of the expression of p70S6K1, HIF-1 α , and VEGF. The major organs including heart, liver, spleen, lung, and kidney were collected for H&E histological assay for toxicity evaluation.

Histology and Immunohistochemistry Analysis: Tumors and major organs were fixed with 4% paraformaldehyde and processed for paraffin section. Organ sections were stained with H&E for acute toxicity and organ metastasis evaluation. Tumor vessels were stained using rabbit antimouse CD31 antibody (Abcam, Hong Kong). The expression of the proteins influenced by the miRNA-145 intervention^[6] was stained with specific primary antibodies including rabbit anti-p70S6K1 antibody (Abcam, Hong Kong), rabbit anti-HIF-1 α antibody (Abcam, Hong Kong), and rabbit anti-VEGF antibody (Abcam, Hong Kong). All the images were taken by Leica DFC 320 photomicroscope. MVD and relative percentage of protein expression were analyzed and scored blindly by the pathologists using Image-Pro Plus 6.0 software (Media Cybernetics, Bethesda, MD).

Statistical Analysis: Statistical analysis was conducted using GraphPad Prism 6.0 software (La Jolla, CA). Differences between groups were examined using Student's *t*-test or ANOVA with Tukey's multiple comparison tests. Differences were considered significant if *p*-value was less than 0.05.

Supporting Information

Supporting Information is available from the Wiley Online Library or from the author.

Acknowledgements

This work was supported by National Natural Science Foundation of China (81572998, 81602729, and 81773274), Shanghai Municipal Science and Technology Commission (16520710700), and "Shu Guang" Program of Shanghai Education Development Foundation and Shanghai Municipal Education Commission (16SG13).

Conflict of Interest

The authors declare no conflict of interest.

Keywords

combination treatment, doxorubicin, mesoporous silica nanoparticles, miRNA-145, orthotopic colorectal cancer model

Received: February 10, 2018

Revised: March 17, 2018

Published online: April 30, 2018

- [1] a) W. Fan, B. Yung, P. Huang, X. Chen, *Chem. Rev.* **2017**, *117*, 13566; b) P. Y. Teo, W. Cheng, J. L. Hedrick, Y. Y. Yang, *Adv. Drug Delivery Rev.* **2016**, *98*, 41; c) V. Tsouris, M. K. Joo, S. H. Kim, I. C. Kwon, Y. Y. Won, *Biotechnol. Adv.* **2014**, *32*, 1037.

- [2] M. Khan, Z. Y. Ong, N. Wiradharma, A. B. Attia, Y. Y. Yang, *Adv. Healthcare Mater.* **2012**, *1*, 373.

- [3] Y. Chen, H. Chen, J. Shi, *Mol. Pharm.* **2014**, *11*, 2495.
- [4] a) O. Taratula, O. B. Garbuzenko, A. M. Chen, T. Minko, *J. Drug Target.* **2011**, *19*, 900; b) M. Wu, Q. Meng, Y. Chen, L. Zhang, M. Li, X. Cai, Y. Li, P. Yu, L. Zhang, J. Shi, *Adv. Mater.* **2016**, *28*, 1963; c) H. Meng, M. Liong, T. Xia, Z. Li, Z. Ji, J. I. Zink, A. E. Nel, *ACS Nano* **2010**, *4*, 4539; d) H. Meng, W. X. Mai, H. Zhang, M. Xue, T. Xia, S. Lin, X. Wang, Y. Zhao, Z. Ji, J. I. Zink, A. E. Nel, *ACS Nano* **2013**, *7*, 994.
- [5] M. Hussain, G. Beale, M. Hughes, S. Akhtar, *Int. J. Pharm.* **2002**, *234*, 129.
- [6] a) T. Xia, M. Kovochich, M. Liong, H. Meng, S. Kabehie, S. George, J. I. Zink, A. E. Nel, *ACS Nano* **2009**, *3*, 3273; b) H. Meng, M. Xue, T. Xia, Z. Ji, D. Y. Tarn, J. I. Zink, A. E. Nel, *ACS Nano* **2011**, *5*, 4131.
- [7] M. Y. Hanafi-Bojd, M. R. Jaafari, N. Ramezani, K. Abnous, B. Malaekhe-Nikouei, *Curr. Drug Delivery* **2016**, *13*, 1176.
- [8] X. Ma, Y. Zhao, K. W. Ng, Y. Zhao, *Chemistry* **2013**, *19*, 15593.
- [9] J. Shen, H. Liu, C. Mu, J. Wolfram, W. Zhang, H. C. Kim, G. Zhu, Z. Hu, L. N. Ji, X. Liu, M. Ferrari, Z. W. Mao, H. Shen, *Nanoscale* **2017**, *9*, 5329.
- [10] Y. Gao, Y. Chen, X. Ji, X. He, Q. Yin, Z. Zhang, J. Shi, Y. Li, *ACS Nano* **2011**, *5*, 9788.
- [11] Y. Chen, H. Chen, D. Zeng, Y. Tian, F. Chen, J. Feng, J. Shi, *ACS Nano* **2010**, *4*, 6001.
- [12] Y. Wang, K. Zhou, G. Huang, C. Hensley, X. Huang, X. Ma, T. Zhao, B. D. Sumer, R. J. DeBerardinis, J. Gao, *Nat. Mater.* **2014**, *13*, 204.
- [13] A. E. Nel, L. Madler, D. Velegol, T. Xia, E. M. Hoek, P. Somasundaran, F. Klaessig, V. Castranova, M. Thompson, *Nat. Mater.* **2009**, *8*, 543.
- [14] a) M. Talelli, M. Barz, C. J. Rijcken, F. Kiessling, W. E. Hennink, T. Lammers, *Nano Today* **2015**, *10*, 93; b) Y. Lu, A. A. Aimetti, R. Langer, Z. Gu, *Nat. Rev. Mater.* **2016**, <https://doi.org/10.1038/natrevmats.2016.14>.
- [15] Y. Chen, D. Y. Gao, L. Huang, *Adv. Drug Delivery Rev.* **2015**, *81*, 128.
- [16] Q. Xu, L. Z. Liu, X. Qian, Q. Chen, Y. Jiang, D. Li, L. Lai, B. H. Jiang, *Nucleic Acids Res.* **2012**, *40*, 761.
- [17] a) F. Loupakis, C. Cremolini, G. Masi, S. Lonardi, V. Zagonel, L. Salvatore, E. Cortesi, G. Tomasello, M. Ronzoni, R. Spadi, A. Zaniboni, G. Tonini, A. Buonadonna, D. Amoroso, S. Chiara, C. Carlomagno, C. Boni, G. Allegri, L. Boni, A. Falcone, *N. Engl. J. Med.* **2014**, *371*, 1609; b) E. Esin, S. Yalcin, *Cancer Treat. Rev.* **2016**, *42*, 82.
- [18] M. A. Arap, J. Lahdenranta, P. J. Mintz, A. Hajitou, A. S. Sarkis, W. Arap, R. Pasqualini, *Cancer Cell* **2004**, *6*, 275.
- [19] Z. Li, L. Zhang, Y. Zhao, H. Li, H. Xiao, R. Fu, C. Zhao, H. Wu, Z. Li, *Int. J. Biochem. Cell Biol.* **2013**, *45*, 987.
- [20] D. Xiao, H. Z. Jia, J. Zhang, C. W. Liu, R. X. Zhuo, X. Z. Zhang, *Small* **2014**, *10*, 591.
- [21] U. Lachelt, E. Wagner, *Chem. Rev.* **2015**, *115*, 11043.
- [22] a) Q. Sun, X. Sun, X. Ma, Z. Zhou, E. Jin, B. Zhang, Y. Shen, E. A. Van Kirk, W. J. Murdoch, J. R. Lott, T. P. Lodge, M. Radosz, Y. Zhao, *Adv. Mater.* **2014**, *26*, 7615; b) Q. Sun, Z. Zhou, N. Qiu, Y. Shen, *Adv. Mater.* **2017**, *29*, 1606628.
- [23] L. Pan, Q. He, J. Liu, Y. Chen, M. Ma, L. Zhang, J. Shi, *J. Am. Chem. Soc.* **2012**, *134*, 5722.
- [24] K. Tewey, T. Rowe, L. Yang, B. Halligan, L. Liu, *Science* **1984**, *226*, 466.
- [25] R. Cheng, F. Feng, F. Meng, C. Deng, J. Feijen, Z. Zhong, *J. Controlled Release* **2011**, *152*, 2.
- [26] a) R. Hong, G. Han, J. M. Fernández, B.-J. Kim, N. S. Forbes, V. M. Rotello, *J. Am. Chem. Soc.* **2006**, *128*, 1078; b) H. Kim, S. Kim, C. Park, H. Lee, H. J. Park, C. Kim, *Adv. Mater.* **2010**, *22*, 4280.
- [27] a) S. Chatterjee, L. C. Heukamp, M. Siobal, J. Schottle, C. Wiczorek, M. Peifer, D. Frasca, M. Koker, K. König, L. Meder, D. Rauh, R. Buettner, J. Wolf, R. A. Brekken, B. Neumaier,

- G. Christofori, R. K. Thomas, R. T. Ullrich, *J. Clin. Invest.* **2013**, *123*, 1732; b) S. Guo, L. S. Colbert, M. Fuller, Y. Zhang, R. R. Gonzalez-Perez, *Biochim. Biophys. Acta* **2010**, *1806*, 108.
- [28] a) Q. Lin, C. S. Jin, H. Huang, L. Ding, Z. Zhang, J. Chen, G. Zheng, *Small* **2014**, *10*, 3072; b) C. S. Jin, H. Wada, T. Anayama, P. Z. McVeigh, H. P. Hu, K. Hirohashi, T. Nakajima, T. Kato, S. Keshavjee, D. Hwang, B. C. Wilson, G. Zheng, K. Yasufuku, *Cancer Res.* **2016**, *76*, 5870.
- [29] C. Hackl, S. Man, G. Francia, C. Milsom, P. Xu, R. S. Kerbel, *Gut* **2013**, *62*, 259.
- [30] Y. L. Tsai, Y. Zhang, C. C. Tseng, R. Stanciauskas, F. Pinaud, A. S. Lee, *J. Biol. Chem.* **2015**, *290*, 8049.
- [31] a) U. Leung, M. Gonen, P. J. Allen, T. P. Kingham, R. P. DeMatteo, W. R. Jarnagin, M. I. D'Angelica, *Ann. Surg.* **2017**, *265*, 158; b) E. Van Cutsem, A. Cervantes, B. Nordlinger, D. Arnold, *Ann. Oncol.* **2014**, *25*, iii1.
- [32] J. S. Tomlinson, W. R. Jarnagin, R. P. DeMatteo, Y. Fong, P. Kornprat, M. Gonen, N. Kemeny, M. F. Brennan, L. H. Blumgart, M. D'Angelica, *J. Clin. Oncol.* **2007**, *25*, 4575.
- [33] a) S. M. Weis, D. A. Cheresh, *Nat. Med.* **2011**, *17*, 1359; b) H. H. Lai, J. N. Li, M. Y. Wang, H. Y. Huang, C. M. Croce, H. L. Sun, Y. J. Lyu, J. W. Kang, C. F. Chiu, M. C. Hung, H. I. Suzuki, P. S. Chen, *J. Clin. Invest.* **2018**, *128*, 625.
- [34] J. E. Lee, N. Lee, H. Kim, J. Kim, S. H. Choi, J. H. Kim, T. Kim, I. C. Song, S. P. Park, W. K. Moon, T. Hyeon, *J. Am. Chem. Soc.* **2010**, *132*, 552.
- [35] B. Chang, D. Chen, Y. Wang, Y. Chen, Y. Jiao, X. Sha, W. Yang, *Chem. Mater.* **2013**, *25*, 574.
- [36] M. H. Lee, Z. Yang, C. W. Lim, Y. H. Lee, S. Dongbang, C. Kang, J. S. Kim, *Chem. Rev.* **2013**, *113*, 5071.
- [37] D. W. Dong, S. W. Tong, X. R. Qi, *J. Biomed. Mater. Res., Part A* **2013**, *101*, 1336.
- [38] L. Zhu, R. I. Mahato, *Bioconjugate Chem.* **2010**, *21*, 2119.
- [39] S. P. Kasturi, K. Sachaphibulkij, K. Roy, *Biomaterials* **2005**, *26*, 6375.
- [40] M. M. van Schooneveld, E. Vucic, R. Koole, Y. Zhou, J. Stocks, D. P. Cormode, C. Y. Tang, R. E. Gordon, K. Nicolay, A. Meijerink, Z. A. Fayad, W. J. Mulder, *Nano Lett.* **2008**, *8*, 2517.